

Radiology Workflow-Guided Hierarchical Reinforcement Fine-Tuning for Medical Report Generation

Bodong Du¹, Honglong Yang¹, and Xiaomeng Li^{1,*}

¹Department of Electronic and Computer Engineering,
Hong Kong University of Science and Technology, Hong Kong, SAR, China
{bduag, hyangdh}@connect.ust.hk, eexmli@ust.hk

November 14, 2025

Abstract

Radiologists compose diagnostic reports through a structured workflow: they describe visual findings, summarize them into impressions, and carefully refine statements in clinically critical cases. However, most existing medical report generation (MRG) systems treat reports as flat sequences, overlooking this hierarchical organization and leading to inconsistencies between descriptive and diagnostic content. To align model behavior with real-world reporting practices, we propose **RadFlow**, a hierarchical workflow-guided reinforcement optimization framework that explicitly models the structured nature of clinical reporting. RadFlow introduces a clinically grounded reward hierarchy that mirrors the organization of radiological reports. At the **global level**, the reward integrates linguistic fluency, medical-domain correctness, and cross-sectional consistency between Finding and Impression, promoting coherent and clinically faithful narratives. At the **local level**, a section-specific reward emphasizes Impression quality, reflecting its central role in diagnostic accuracy. Furthermore, a **critical-aware policy optimization** mechanism adaptively regularizes learning for high-risk or clinically sensitive cases, emulating the cautious refinement behavior of radiologists when documenting critical findings. Together, these components translate the structured reporting paradigm into the reinforcement fine-tuning process, enabling the model to generate reports that are both linguistically consistent and clinically aligned. Experiments on carotid ultrasound and chest X-ray datasets demonstrate that RadFlow consistently improves diagnostic coherence and overall report quality compared with state-of-the-art baselines.

Keywords: Medical Report Generation, Reinforcement Fine-Tuning, Hierarchical Reward, Structured Reporting, Diagnostic Accuracy

*Corresponding author: Xiaomeng Li.

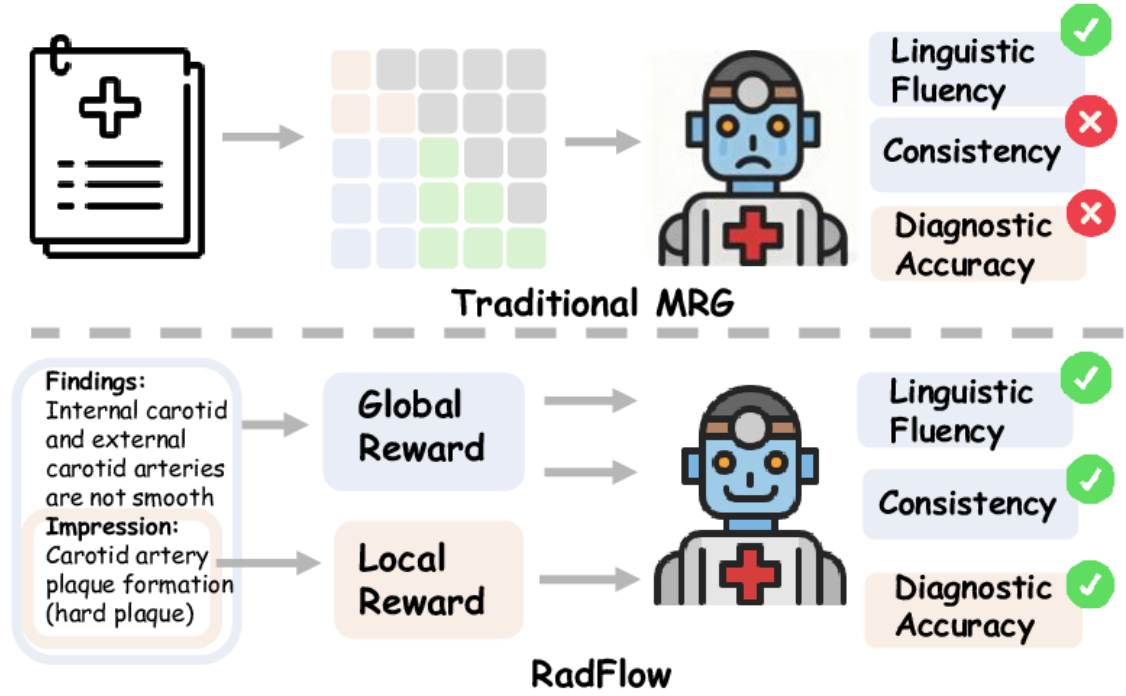


Figure 1: Conceptual illustration of **RadFlow**. Traditional models treat reports as flat token sequences, ignoring the structured logic between *Findings* and *Impression*. RadFlow introduces hierarchical rewards, where the **global reward** enforces descriptive and cross-sectional consistency, and the **local reward** enhances diagnostic reasoning.

1 Introduction

Radiologists compose diagnostic reports through a structured and hierarchical process [1, 2]. They first describe image-level observations and visual cues in the *Findings* section, then summarize these into diagnostic conclusions in the *Impression* section, and finally refine their statements when encountering clinically critical or uncertain cases. This structured workflow ensures logical consistency between descriptive observations and diagnostic judgments, enabling both readability and clinical accountability in real-world practice. Replicating this logical and hierarchical workflow remains a major challenge for AI systems.

Early Medical Report Generation (MRG) systems [3–9] laid the foundation for automatic report generation. More recently, multimodal large language models (MLLMs) such as R2GenGPT [10], RaDialog [11], and MedVersa [12] have achieved significant progress by leveraging large-scale supervised fine-tuning on paired image-report datasets. However, these methods commonly overlook the inherent hierarchical structure of reports and treat the report text as a flat sequence, as illustrated in Figure 1. As a result, they often generate syntactically fluent narratives that are clinically inconsistent, for example by omitting critical pathologies such as “hard plaque” or introducing incorrect terms such as “mixed plaque,” even when these entities appear inconsistently elsewhere in the generated report (see “MedVersa” results in Figure 3).

To bridge this gap, we propose **RadFlow**, a reinforcement fine-tuning framework that explicitly aligns model learning dynamics with the structured reporting process of radiologists. In clinical practice, radiologists follow a hierarchical workflow consisting of three cognitive actions:

(1) *describing* visual observations in the *Findings* section, (2) *interpreting* them into diagnostic conclusions in the *Impression*, and (3) *refining* statements in clinically critical or uncertain cases. RadFlow translates these human-level actions into a reward-driven learning hierarchy, enabling the model to emulate this structured diagnostic reasoning process. At the **global level**, the reward corresponds to the radiologist’s *descriptive synthesis* behavior, which assesses whether the report is linguistically fluent, diagnostic accuracy, and semantically consistent across sections. In particular, this level incorporates a **cross-sectional consistency reward** that evaluates whether the *Impression* faithfully summarizes and logically aligns with the *Findings*, thereby reflecting the physician’s internal verification between descriptive and diagnostic content. At the **local level**, the reward captures the *diagnostic interpretation* action, directly evaluating the accuracy and completeness of the *Impression* section, which encapsulates the physician’s diagnostic process. Finally, the **critical-aware policy optimization** mirrors the *refinement* behavior of radiologists when documenting high-risk or clinically sensitive findings. It adaptively regularizes policy updates in such cases to ensure stability and cautious optimization. By explicitly mapping each reward component to a corresponding clinical action, RadFlow bridges the gap between medical reporting process and model optimization. This alignment allows the model to generate reports that follow the same structured workflow as human experts, including observing, describing, and refining, resulting in narratives that are both clinically faithful and diagnostically consistent.

Extensive experiments on carotid ultrasound and chest X-ray benchmarks [13–15] demonstrate that RadFlow achieves superior diagnostic consistency, sectional alignment, and overall report quality compared with state-of-the-art baselines. Beyond performance improvement, this study highlights a promising direction for bridging reinforcement optimization with structured clinical reporting, translating medical workflow principles into model learning dynamics.

To summarize, this work makes the following contributions:

- We formulate **RadFlow**, a workflow-guided reinforcement fine-tuning framework that aligns report generation with the hierarchical diagnostic process of radiologists.
- We design a **clinical-aware hierarchical reward** that captures both global report coherence and local diagnostic accuracy, explicitly bridging descriptive and interpretive process.
- We demonstrate through extensive experiments on carotid ultrasound and chest X-ray datasets that **RadFlow** substantially improves diagnostic consistency and clinical interpretability over state-of-the-art MRG baselines.

2 Related Work

2.1 Medical Report Generation

MRG [3,4] is a critical yet challenging clinical AI task that demands precise alignment between imaging findings and diagnostic interpretations. Significant progress has been made in report quality and clinical fidelity through various innovations [6,7,16–21]. The rise of multimodal large language models (MLLMs) [22,23], with their strong cross-modal understanding, has further accelerated MRG research. Recent works [24–27] adapt general-purpose foundation models to

medicine via supervised fine-tuning like R2GenGPT [10], RaDialog [11], MedVersa [12] and RADAR [28].

MedVersa serves as a strong generalist MRG foundation but relies on surface-level supervision and struggles to produce structured diagnostic summaries, especially in the clinically vital *Impression* section. RADAR improves factual consistency in *Findings* by fusing internal knowledge and external retrieval, yet its retrieval-driven design lacks effective abstract summarization, resulting in incoherent or inaccurate *impressions*. This underscores a key limitation of current approaches: the inability to bridge image-level observations with diagnostic-level synthesis in a controllable, end-to-end manner.

2.2 Reinforcement Fine-Tuning

Recent advances in reinforcement fine-tuning (RFT) have significantly improved large reasoning models across domains. Visual-RFT extends RFT to vision-language tasks using verifiable rewards (e.g., IoU) and GRPO, achieving gains in fine-grained classification and detection [29]. MM-EUREKA enhances multimodal mathematical reasoning via rule-based RL with stable training and diverse data [30]. DAPO improves reproducibility through Decoupled Clip and Dynamic Sampling Policy Optimization, setting state-of-the-art results on Qwen2.5-32B [31]. GSPO boosts RL stability and efficiency via sequence-level importance weighting, advancing models like Qwen3 [32]. Building on these, recent medical works adapt RFT to clinical tasks with limited success. AlphaMed [33] and Med-U1 [34] demonstrate RFT benefits in multiple-choice medical reasoning under constrained rewards. Vision-language methods like MedVLM [35] and Med-R1 [36] apply GRPO without supervised fine-tuning, excelling in visual QA but struggling with long-form clinical narratives.

Although reinforcement learning (RL) and RL with human feedback (RLHF) have been applied to MRG [37, 38], none have leveraged RFT. To our knowledge, RadFlow is the first to apply RFT to long-form medical report generation. Notably, LHR-RFL [39] uses RL with a hybrid reward but focuses primarily on hard sample mining, lacks explicit hierarchical modeling of clinical reports, and fails to generate high-fidelity *Findings* section. This limitation undermines cross-sectional consistency between *Finding* and *Impression*. In contrast, RadFlow introduces fine-grained hierarchical reward modeling that jointly optimizes linguistic fluency, section-wise diagnostic accuracy, and global narrative coherence.

3 Preliminary

3.1 Problem Formulation

MRG aims to translate medical images into structured, clinically coherent text. Unlike general image captioning, MRG follows domain-specific conventions typically comprising two parts: **Finding** (visual observations) and **Impression** (diagnostic summaries).

Formally, given input image(s) x_i , optional prior image x_i^p , and clinical context c_i (e.g., indication or history), the goal is to generate a report $y_i = \{y_{i,1}, \dots, y_{i,T}\}$, where $y_{i,t}$ denotes the t -th token of the report.

A vision large language model (VLLM), combining a vision encoder, connector (e.g., Q-Former), and LLM, models the conditional token distribution:

$$p(y_{i,t} \mid x_i, x_i^p, c_i, y_{i,<t}).$$

The model is trained to maximize the likelihood of the report sequence, aligning generated outputs with domain-specific reporting structure and semantics.

3.2 Group Relative Policy Optimization

Group Relative Policy Optimization (GRPO) is a reinforcement fine-tuning algorithm designed to train large language models using group-based feedback without relying on an explicit value function. Given a question-answer pair (q, a) , the behavior policy π_{old} samples a group of G candidate responses $\{o_i\}_{i=1}^G$, each assigned a scalar reward r_i derived from rule-based or preference-based heuristics.

To assess relative response quality, GRPO normalizes rewards within each group:

$$\hat{A}_{i,t} = \frac{r_i - \text{mean}(\{r_j\}_{j=1}^G)}{\text{std}(\{r_j\}_{j=1}^G)}. \quad (1)$$

Token-level importance weight is computed as:

$$r_{i,t}(\theta) = \frac{\pi_{\theta}(o_{i,t} \mid q, o_{i,<t})}{\pi_{\text{old}}(o_{i,t} \mid q, o_{i,<t})}. \quad (2)$$

The training objective encourages models to upweight responses with above-average rewards while preventing policy collapse through clipped updates:

$$\mathcal{J}_{\text{GRPO}}(\theta) = \mathbb{E}_{(q,a) \sim D, \{o_i\}_{i=1}^G \sim \pi_{\text{old}}(\cdot \mid q)} \left[\frac{1}{G} \sum_{i=1}^G \frac{1}{|o_i|} \sum_{t=1}^{|o_i|} \min \left(r_{i,t}(\theta) \hat{A}_{i,t}, \text{clip}(r_{i,t}(\theta), 1-\epsilon, 1+\epsilon) \hat{A}_{i,t} - \beta D_{KL}(\pi_{\theta} \parallel \pi_{\text{ref}}) \right) \right] \quad (3)$$

This formulation removes the need for explicit reward models and scales well with group-wise preference signals, making it suitable for instruction tuning and alignment tasks.

4 Method

We propose RadFlow, a reinforcement fine-tuning framework that aligns model learning with the structured diagnostic workflow of radiologists. Our approach begins with **supervised fine-tuning (SFT)** to align a pretrained vision-language model with domain-specific reporting conventions as a reference model. Building on this foundation, we introduce **hierarchical alignment reinforcement fine-tuning**, which optimizes a clinically grounded reward structure that mirrors two key aspects of radiologists’ workflow: (1) *descriptive synthesis*, which ensures global coherence and cross-sectional consistency between Finding and Impression, and (2) *diagnostic interpretation*, which focuses on Impression-level accuracy. This optimization is performed via **critical-aware policy optimization**, which adaptively regularizes learning

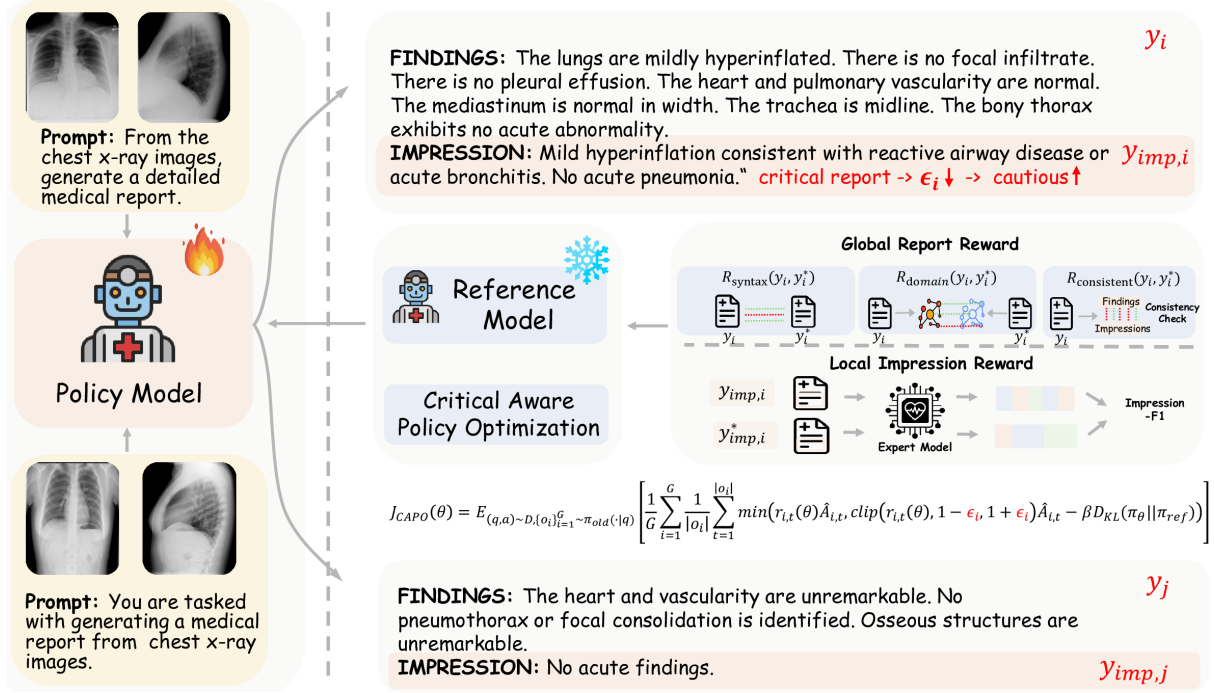


Figure 2: Overview of the RadFlow framework, which translates radiologists’ structured reporting workflow into reinforcement fine-tuning. Given an image and prompt, the **Policy Model** generates candidate reports (e.g., y_i, y_j). A **hierarchical reward** guides optimization: (1) *Global Report Reward* jointly evaluates linguistic fluency, domain correctness, and cross-sectional consistency between Finding and Impression; (2) *Local Impression Reward* prioritizes diagnostic accuracy in the critical Impression section via an expert model. The **Critical-Aware Policy Optimization** module adaptively adjusts learning for high-risk cases (e.g., $\epsilon_i \downarrow \rightarrow$ cautious \uparrow), mimicking radiologists’ careful refinement under clinical uncertainty.

for clinically critical cases and emulates the cautious refinement behavior of radiologists when documenting high-stakes findings.

4.1 Overall Pipeline

Given a training dataset $\mathcal{D} = \{(x_i, y_i^*)\}_{i=1}^N$, we first perform supervised fine-tuning (SFT) to obtain a reference model $\pi_{\theta}^{\text{SFT}}$. While $\pi_{\theta}^{\text{SFT}}$ generally yields fluent outputs, some training examples still exhibit diagnostic errors or inconsistencies between the *Findings* and *Impression* sections. To concentrate reinforcement optimization on these diagnostically challenging cases, we introduce a targeted selection pipeline (Target Exploration) that proceeds as follows.

1. **Predict on training set.** For each training input x_i , produce a predicted report $y_i = \pi_{\theta}^{\text{SFT}}(x_i)$.

2. **Compute composite ranking score.** Evaluate each prediction y_i using a set of complementary metrics capturing surface fluency, semantic fidelity, and clinical correctness (e.g., BLEU-2 [40], BERTScore [41], and RadGraph [42]). These metric values are combined into a single consistency–fidelity score

$$s_i = \mathcal{S}(\text{BLEU2}(y_i), \text{BERTScore}(y_i), \text{RadGraph}(y_i)),$$

where $\mathcal{S}(\cdot)$ denotes a normalized aggregation function (e.g., weighted sum after metric-specific normalization).

3. Rank and select hard examples. Rank samples by s_i in ascending order and select the lowest-scoring subset $\tilde{\mathcal{D}} = \{(x_j, y_j^*)\}_{j \in \mathcal{I}}$ (e.g., the bottom- $k\%$ or those with $s_i < \tau$ for a threshold τ). This subset contains examples where SFT outputs deviate most from expected clinical content and are therefore most likely to benefit from targeted reinforcement optimization.

4. Reinforcement optimization on the selected subset. Apply reinforcement fine-tuning only on $\tilde{\mathcal{D}}$, using the proposed **Hierarchical Alignment Reward** to enforce cross-sectional consistency (global + local rewards) and **CAPO** (Critical-Aware Policy Optimization) to adaptively regularize learning on clinically sensitive cases, as illustrated in Figure 2. Restricting RL updates to $\tilde{\mathcal{D}}$ concentrates computational effort on problematic samples while preserving well-formed SFT outputs on the remainder of the training set.

This Target Exploration procedure therefore directs hierarchical reward signals and CAPO to the most diagnostically informative samples, improving clinical consistency and diagnostic accuracy without degrading general linguistic fluency learned during SFT.

4.2 Hierarchical Alignment Reward

Inspired by radiologists’ structured reporting workflow, where they first *describe* visual observations in the *Findings* section and then *interpret* them into diagnostic conclusions in the *Impression*, we design a **hierarchical alignment reward** that explicitly models this two-stage cognitive process. The total reward is decomposed as:

$$R(y_i) = R_{\text{global}}(y_i) + \gamma R_{\text{imp}}(y_{\text{imp},i}), \quad (4)$$

where:

Global Report Reward $R_{\text{global}}(y_i)$ captures the radiologist’s *descriptive synthesis* behavior and is further decomposed as:

$$R_{\text{global}}(y_i) = R_{\text{syntax}}(y_i) + R_{\text{domain}}(y_i) + R_{\text{consistent}}(y_i), \quad (5)$$

with $R_{\text{syntax}}(y_i)$: linguistic fluency (e.g., BLEU, ROUGE-L), $R_{\text{domain}}(y_i)$: medical correctness of the *Findings* (e.g., RadGraph), $R_{\text{consistent}}(y_i)$: cross-sectional consistency between *Findings* and *Impression*. Crucially, R_{cons} is implemented via an LLM-as-a-judge paradigm: we prompt GPT-4o [43] with the generated *Findings* and *Impression* and ask whether the diagnostic conclusion logically follows from the observations. The response is binarized:

$$R_{\text{consistent}}(y_i) = \begin{cases} +1, & \text{if consistent,} \\ -1, & \text{otherwise.} \end{cases}$$

This ensures the model is explicitly rewarded for maintaining internal logical coherence which is the hallmark of expert reporting.

Local Impression Reward $R_{\text{imp}}(y_{\text{imp},i})$ ensures accuracy of the Impression section. A

pretrained Expert model (e.g., CheXpert) predicts label probabilities:

$$\hat{\mathbf{p}}_i = \text{Expert}(y_{\text{imp},i}), \quad \mathbf{p}_i^* = \text{Expert}(y_{\text{imp},i}^*), \quad (6)$$

which are binarized and compared via macro F1:

$$R_{\text{imp}}(y_{\text{imp},i}) = \text{F1}(\text{Binarize}(\hat{\mathbf{p}}_i), \text{Binarize}(\mathbf{p}_i^*)). \quad (7)$$

The deterministic section parser identifies **findings** and **Impression** sections. If headers are missing or ambiguous, the full report contributes to R_{global} , while R_{imp} is skipped, preventing misaligned reinforcement. This hierarchical separation justifies the term *alignment*: it explicitly aligns model outputs to both global fluency patterns and critical diagnostic elements.

4.3 Critical-Aware Policy Optimization

To emulate the nuanced diagnostic behavior of radiologists, who allocate greater cognitive effort and exercise heightened caution when documenting clinically critical or abnormal findings, we propose a **critical-aware policy optimization** (CAPO) mechanism. This approach introduces an adaptive learning constraint that dynamically modulates the strength of policy updates based on the clinical criticality of each case, mirroring the *refinement* stage of radiologists’ reporting workflow.

Formally, we modify the standard GRPO objective by incorporating a case-dependent clipping range ϵ_i , yielding the CAPO objective:

$$\begin{aligned} \mathcal{J}_{\text{CAPO}}(\theta) = & \mathbb{E}_{(q,a) \sim D, \{o_i\}_{i=1}^G \sim \pi_{\text{old}}(\cdot|q)} \left[\frac{1}{G} \sum_{i=1}^G \frac{1}{|o_i|} \sum_{t=1}^{|o_i|} \right. \\ & \left. \min \left(r_{i,t}(\theta) \hat{A}_{i,t}, \text{clip}(r_{i,t}(\theta), 1 - \epsilon_i, 1 + \epsilon_i) \hat{A}_{i,t} - \beta D_{KL}(\pi_\theta \| \pi_{\text{ref}}) \right) \right] \end{aligned} \quad (8)$$

Here, the clipping range ϵ_i is adaptively set according to the clinical criticality of the reference report y_i^* :

$$\epsilon_i = \begin{cases} \epsilon_{\text{critical}} = \frac{\epsilon_{\text{normal}}}{4}, & \text{if } y_i^* \text{ is critical,} \\ \epsilon_{\text{normal}}, & \text{otherwise.} \end{cases} \quad (9)$$

Crucially, the criticality of each report is pre-annotated *before training* using GPT-4o as an expert clinical judge. Specifically, we prompt GPT-4o with the reference report and ask: “Does this report describe any abnormal, pathological, or clinically significant finding?” Responses are binarized: reports explicitly stating “no significant findings” or equivalent are labeled *normal*; all others are labeled *critical*. This LLM-based triage ensures broad and flexible coverage across diverse pathologies without reliance on fixed label sets or domain-specific classifiers.

By tightening the policy update bound ($\epsilon_{\text{critical}} < \epsilon_{\text{normal}}$) for critical cases, CAPO enforces more conservative optimization, reducing the risk of aggressive, hallucinated revisions in high-stakes scenarios. This directly mimics radiologists’ cautious refinement behavior: stable, deliberate updates when diagnostic certainty is low or clinical impact is high, and more exploratory learning for routine cases. In this way, CAPO embeds real-world clinical reasoning

into the reinforcement fine-tuning dynamics, ensuring both safety and adaptability.

4.4 Theoretical Analysis of Critical-Aware Policy Optimization

To justify the design of CAPO, we analyze its policy stability under case-dependent clipping. Consider an Markov Decision Process with bounded reward $|r(s, a)| \leq R_{\max}$ and discount factor $\gamma \in (0, 1)$. Under standard assumptions (e.g., $\pi_{\text{old}}(a|s) > 0$), the following holds:

Lemma (Policy Smoothness). If the probability ratio $r_t(\theta) = \pi_\theta(a|s)/\pi_{\text{old}}(a|s)$ is clipped within $[1 - \epsilon_i, 1 + \epsilon_i]$, then the L1 distance between policies is bounded by:

$$\max_s \|\pi_\theta(\cdot|s) - \pi_{\text{old}}(\cdot|s)\|_1 \leq \epsilon_i.$$

Proposition (Return Stability). The change in expected return is bounded as:

$$|J(\pi_\theta) - J(\pi_{\text{old}})| \leq \frac{2R_{\max}}{(1 - \gamma)^2} \epsilon_i.$$

These results imply that by setting $\epsilon_i = \epsilon_{\text{critical}} \ll \epsilon_{\text{normal}}$ for clinically critical reports, CAPO enforces tighter policy updates and smoother learning trajectories on high-stakes cases. This adaptive mechanism thus provides a provable guarantee that aligns optimization behavior with radiologists’ cautious refinement practice, conservative updates when clinical risk is high, flexible learning otherwise, without sacrificing overall training efficiency.

5 Experiments

In this section, we evaluate the effectiveness of our proposed method on two different modality datasets obtained from clinical practice. The qualitative results demonstrate that RadFlow generates higher quality medical reports compared to existing methods.

5.1 Datasets

We evaluate our model on four datasets covering different imaging modalities: CarotidUS-MRG: A private dataset of 12,000 carotid ultrasound studies with expert-annotated reports, split by patient (70/15/15%) to prevent leakage. Reports follow a standardized format for structured clinical documentation. MIMIC-CXR [14]: A public chest X-ray dataset with 377,110 frontal images and 227,827 associated reports. IU-Xray [13]: A public chest X-ray dataset with 8,121 images and 7,470 reports from 3,955 patients. ReXGradient-160K [15]: The largest publicly available multi-site chest X-ray dataset, containing 273,004 images from 160,000 radiological studies across 109,487 patients from 79 medical sites. And we adopt the official split for consistency with prior studies [44] enabling direct comparison with existing work.

5.2 Experimental Setup

Evaluation Metrics. We assess model performance using both standard natural language generation (NLG) metrics and clinically grounded metrics. BLEU [40], BERTScore [41], and SemScore [5] are used to evaluate general linguistic quality. For the MIMIC-CXR, IU-Xray and RexGradient benchmark, we follow the RexRank [44] protocol, incorporating RadGraph

Model	Params (B)	Data (M)	BLEU-2 \uparrow	BERTScore \uparrow	SembScore \uparrow	Keyword \uparrow	BLEU-2 \uparrow	BERTScore \uparrow	SembScore \uparrow	RadGraph \uparrow	1/RadCliQ-v1 \uparrow
			CarotidUS-MRG				MIMIC-CXR				
RadFlow (Ours)	3	0.8	0.522	0.915	0.891	0.742	<u>0.196</u>	0.401	0.442	<u>0.252</u>	0.939
MedVersa [12]	7	30	<u>0.473</u>	<u>0.868</u>	<u>0.837</u>	<u>0.593</u>	0.193	0.430	0.315	0.273	<u>0.919</u>
R2GenGPT [10]	7	0.8	0.453	0.844	0.815	0.589	0.203	0.407	0.305	0.243	0.909
CheXpert-CheX-MIMIC [18]	0.1	0.7	0.458	0.846	0.812	0.571	0.196	<u>0.389</u>	<u>0.429</u>	0.166	0.838
CheXpert-MIMIC [18]	0.1	0.4	0.434	0.818	0.801	0.548	0.165	0.353	0.382	0.193	0.802
CheXpert-CheX [18]	0.1	0.3	0.406	0.801	0.794	0.527	0.127	0.300	0.342	0.173	0.715
RadFM [46]	14	16	0.466	0.856	0.822	0.588	0.081	0.281	0.245	0.111	0.625

Table 1: Cross-dataset evaluation of medical report generation models on CarotidUS-MRG and MIMIC-CXR. Bold = best, underline = second-best.

Model	Params (B)	Data (M)	BLEU-2 \uparrow	BERTScore \uparrow	SembScore \uparrow	RadGraph \uparrow	1/RadCliQ-v1 \uparrow	BLEU-2 \uparrow	BERTScore \uparrow	SembScore \uparrow	RadGraph \uparrow	1/RadCliQ-v1 \uparrow
			IU-xray					ReXGradient				
RadFlow (Ours)	3	0.8	0.284	0.607	0.626	0.313	2.325	0.298	0.544	0.492	0.299	1.45
MedVersa [12]	7	30	0.251	<u>0.579</u>	<u>0.611</u>	<u>0.274</u>	<u>1.852</u>	<u>0.266</u>	<u>0.481</u>	<u>0.488</u>	<u>0.249</u>	<u>1.17</u>
R2GenGPT [10]	7	0.8	<u>0.271</u>	0.558	0.601	0.269	1.751	0.251	0.478	0.479	0.231	1.05
CheXpert-CheX-MIMIC [18]	0.1	0.7	0.264	0.516	0.608	0.257	1.619	0.238	0.437	0.463	0.208	1.038
CheXpert-MIMIC [18]	0.1	0.4	0.257	0.489	0.601	0.232	1.414	0.207	0.394	0.451	0.189	0.961
CheXpert-CheX [18]	0.1	0.3	0.211	0.437	0.572	0.227	1.195	0.181	0.362	0.405	0.168	0.818
RadFM [46]	14	16	0.228	0.491	0.589	0.254	1.320	0.176	0.368	0.409	0.151	0.837

Table 2: Cross-dataset evaluation of medical report generation models on IU-xray and ReX-Gradient. Bold = best, underline = second-best.

Configuration	Hierarchical Alignment	Target Exploration	BLEU-2 \uparrow	BERTScore \uparrow	SembScore \uparrow	Keyword \uparrow	BLEU-2 \uparrow	BERTScore \uparrow	SembScore \uparrow	RadGraph \uparrow	1/RadCliQ-v1 \uparrow
			CarotidUS-MRG				MIMIC-CXR				
Base	\times	\times	0.481	0.861	0.865	0.661	0.113	0.296	0.327	0.162	0.699
Hierarchical Alignment Reward	\checkmark	\times	0.498	0.882	0.877	0.691	0.169	0.362	0.388	0.207	0.875
Critical-Aware Policy Optimization	\checkmark	\times	0.489	0.871	0.869	0.678	0.147	0.321	0.342	0.187	0.815
Ours	\checkmark	\checkmark	0.522	0.915	0.891	0.742	0.196	0.401	0.442	0.252	0.939

Table 3: Ablation study of Critical-Aware Policy Optimization and Hierarchical Alignment Reward on the CarotidUS-MRG and MIMIC-CXR dataset.

Configuration	Hierarchical Alignment	Target Exploration	BLEU-2 \uparrow	BERTScore \uparrow	SembScore \uparrow	RadGraph \uparrow	1/RadCliQ-v1 \uparrow	BLEU-2 \uparrow	BERTScore \uparrow	SembScore \uparrow	RadGraph \uparrow	1/RadCliQ-v1 \uparrow
			IU-xray					ReXGradient				
Base	\times	\times	0.253	0.581	0.619	0.289	1.961	0.283	0.531	0.473	0.287	1.33
Hierarchical Alignment Reward	\checkmark	\times	0.274	0.591	0.622	0.305	2.259	0.291	0.540	0.485	0.295	1.392
Critical-Aware Policy Optimization	\checkmark	\times	0.264	0.587	0.620	0.293	2.129	0.288	0.536	0.482	0.291	1.381
Ours	\checkmark	\checkmark	0.284	0.607	0.626	0.313	2.325	0.298	0.544	0.492	0.299	1.453

Table 4: Ablation study of Critical-Aware Policy Optimization and Hierarchical Alignment Reward on the IU-xray and RexGradient dataset.

F1 [42] for structured entity alignment and 1/RadCliQ-v1 [45] for diagnostic coherence. For the CarotidUS-MRG dataset, where RadGraph and RadCliQ-v1 are inapplicable, we introduce KeyWordMatch, a tailored metric based on a proprietary ultrasound report labeler trained in-house on expert-annotated carotid data. It extracts key medical terms from predictions and references, and measures their overlap to assess terminology fidelity. To ensure a fair comparison, we fine-tune MedVersa, CheXpertPlus, and RadFM on the IU-Xray and ReXGradient datasets. **Baselines and Implementation.** We evaluate RadFlow against two categories of baselines: (1) **Public foundation models**, including R2GenGPT [10], MedVersa [12], CheXpertPlus [18], and RadFM [46]; and (2) **Our proposed RadFlow**. All models are trained and evaluated under identical settings, with a learning rate of 1×10^{-5} , LoRA rank of 8, four report generations per case, the bottom-k of 10%, and a batch size of 1. Training consumes approximately 672 GPU-hours on $8 \times$ MetaX C500 GPUs, each equipped with 64GB of VRAM.

5.3 Results on Chest X-ray and Carotid Ultrasound

We first evaluate RadFlow on widely adopted chest X-ray benchmarks to examine its performance on large-scale, clinically diverse datasets. On MIMIC-CXR, RadFlow maintains BLEU-2 comparable to MedVersa while improving semantic alignment, with SembScore increasing from 0.315 to 0.442. More importantly, it achieves the highest clinically-informed 1/RadCliQ-v1,

rising from 0.919 to 0.939 compared to MedVersa, reflecting enhanced consistency between Findings and Impression and improved diagnostic accuracy across diverse pathologies. On IU-Xray, RadFlow continues to outperform baseline methods. BLEU-2 improves from 0.251 to 0.284, SembScore rises from 0.611 to 0.626, and clinically critical alignment as measured by 1/RadCliQ-v1 increases from 1.852 to 2.325, representing an +18.7% gain over MedVersa. These improvements indicate that RadFlow effectively captures complex pathologies and maintains semantic precision, generating reports that closely mirror radiologists’ phrasing. On ReX-Gradient, which covers multi-site, large-scale data, RadFlow demonstrates similar robustness. BLEU-2 increases from 0.266 to 0.298, SembScore rises from 0.488 to 0.492, and 1/RadCliQ-v1 increases from 1.17 to 1.453, representing a +27.5% gain over MedVersa. This confirms that RadFlow consistently preserves diagnostically critical information across heterogeneous imaging conditions.

Extending to carotid ultrasound, RadFlow maintains its advantages on the CarotidUS-MRG dataset. The model achieves the highest semantic alignment and KeywordMatch, with scores increasing from 0.593 to 0.742, representing a +23.6% gain over MedVersa. This demonstrates the model’s capability to capture fine-grained, clinically relevant terminology. These results suggest that the performance gains observed on chest X-ray benchmarks generalize to other imaging modalities, supporting the robustness of RadFlow’s hierarchical reward modeling, critical-aware optimization, and targeted exploration. Collectively, RadFlow consistently generates reports that are fluent, semantically precise, and clinically faithful across both widely studied and specialized imaging domains.

Case Study Figure 3 presents representative case studies comparing the current SOTA MedVersa, our RadFlow model, and expert-annotated reports on the CarotidUS-MRG dataset.

MedVersa tends to generate rather shallow, template-like descriptions, focusing mainly on surface-level features such as intima-media thickness and Doppler flow variations. It frequently overlooks critical clinical indicators like stenosis, hypoechoic photospheres, or subtle echogenic changes, and it occasionally produces an inaccurate or incomplete Impression section. In addition, its language often lacks contextual reasoning, providing a list of measurements without clear connections to the underlying pathology or patient trajectory.

By contrast, RadFlow produces more coherent and informative reports. It integrates multi-modal cues from B-mode and color Doppler frames, combining spatial texture, flow dynamics, and temporal consistency to identify and reason about key pathological features. For instance, while MedVersa may only mention elevated flow velocity or vessel wall irregularity, RadFlow further infers the degree of stenosis, comments on associated hemodynamic consequences, and relates these findings to potential clinical implications. The model also demonstrates greater specificity by differentiating fibrous from calcified plaques, recognizing mixed compositions, and characterizing their stability. It better captures progression patterns over time, highlighting whether changes represent new lesions, chronic remodeling, or rapid plaque growth.

Moreover, the generated impressions produced by RadFlow align closely with expert summaries, offering concise yet comprehensive statements that prioritize salient findings, avoid redundancy, and enhance overall clinical relevance. The model’s outputs are interpretable, allowing clinicians to trace conclusions back to specific imaging features, which supports trust and facilitates decision-making. Additionally, RadFlow shows robustness across diverse pa-

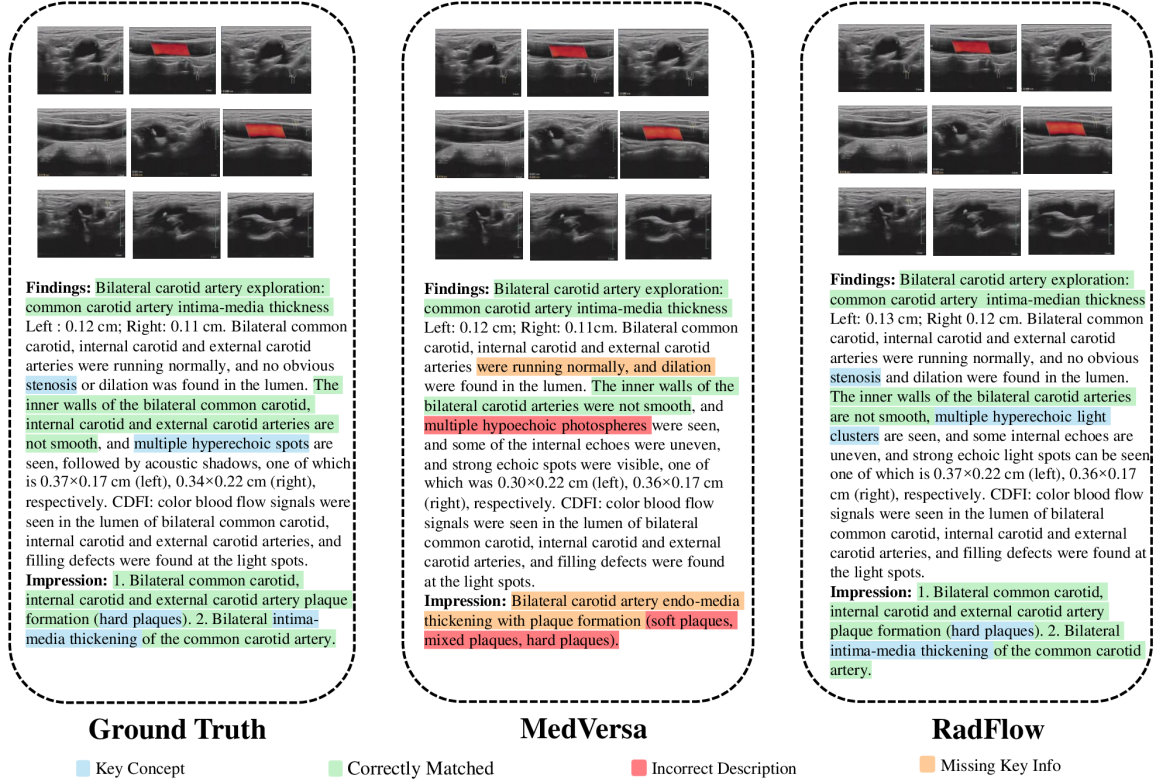


Figure 3: Comparison of generated medical reports under different training strategies. The figure highlights differences in linguistic fluency, diagnostic accuracy, and sectional consistency between MedVersa trained on CarotidUS-MRG and our proposed RadFlow method, demonstrating RadFlow’s superior diagnostic coherence and cross-sectional consistency.

tient cohorts and imaging conditions, suggesting its potential for wider clinical deployment and real-world applicability.

5.4 Ablation Study

We conduct systematic ablation experiments to quantify the individual contributions of hierarchical alignment, target exploration, and the critical-aware optimization design. The experiments are performed on four datasets, namely CarotidUS-MRG, MIMIC-CXR, IU-Xray, and ReXGradient, with results summarized in Table 3 and Table 4. The evaluated model variants include a base supervised model, a model incorporating only the hierarchical alignment reward, a model enhanced with critical-aware policy optimization applied together with hierarchical alignment, and the full RadFlow framework that integrates both hierarchical alignment and target exploration.

Hierarchical alignment consistently improves both linguistic fluency and clinical accuracy. For example, on CarotidUS-MRG, BLEU-2 rises from 0.481 to 0.498 and BERTScore from 0.861 to 0.882, while KeyWordMatch increases from 0.661 to 0.691. Similar trends are observed on MIMIC-CXR, IU-Xray, and ReXGradient, demonstrating that decomposing global fluency and Impression-level correctness into hierarchical rewards effectively strengthens semantic alignment and clinical faithfulness.

CAPO, when applied alongside hierarchical alignment but without target exploration, sta-

Category / Method	Reward / Paradigm	BLEU-2 \uparrow	BERTScore \uparrow	SembScore \uparrow	KeywordMatch \uparrow	BLEU-2 \uparrow	BERTScore \uparrow	SembScore \uparrow	RadGraph \uparrow	1/RadCliQ-v1 \uparrow
		CarotidUS-MRG				MIMIC-CXR				
Ranking Metric	BLEUScore	0.478	0.882	0.874	0.661	0.172	0.342	0.391	0.201	0.831
	BERTScore	0.461	0.867	0.851	0.632	0.163	0.333	0.361	0.182	0.753
	Ours	0.522	0.915	0.891	0.742	0.196	0.401	0.442	0.252	0.939
Training Paradigm	SFT	0.459	0.872	0.859	0.649	0.161	0.321	0.359	0.192	0.902
	RFT	0.522	0.915	0.891	0.742	0.196	0.401	0.442	0.252	0.939
Reward Function	BLEUScore	0.452	0.848	0.841	0.613	0.152	0.342	0.392	0.212	0.883
	BERTScore	0.479	0.879	0.862	0.678	0.171	0.361	0.412	0.223	0.911
	Hierarchical Alignment	0.522	0.915	0.891	0.742	0.196	0.401	0.442	0.252	0.939
Policy Optimization	GRPO	0.491	0.891	0.882	0.664	0.172	0.341	0.383	0.234	0.921
	CAPO	0.522	0.915	0.891	0.742	0.196	0.401	0.442	0.252	0.939

Table 5: Comprehensive evaluation of ranking strategies, training paradigms, reward functions, and policy optimization on CarotidUS-MRG and MIMIC-CXR datasets.

Category / Method	Reward / Paradigm	BLEU-2 \uparrow	BERTScore \uparrow	SembScore \uparrow	RadGraph \uparrow	1/RadCliQ-v1 \uparrow	BLEU-2 \uparrow	BERTScore \uparrow	SembScore \uparrow	RadGraph \uparrow	1/RadCliQ-v1 \uparrow
		IU-Xray					ReXGradient				
Ranking Metric	BLEUScore	0.262	0.583	0.612	0.282	1.962	0.285	0.533	0.474	0.289	1.332
	BERTScore	0.254	0.578	0.605	0.275	1.923	0.290	0.539	0.483	0.292	1.367
	Ours	0.284	0.607	0.626	0.313	2.325	0.298	0.544	0.492	0.299	1.450
Training Paradigm	SFT	0.255	0.579	0.607	0.281	1.930	0.284	0.533	0.476	0.288	1.345
	RFT	0.284	0.607	0.626	0.313	2.325	0.298	0.544	0.492	0.299	1.450
Reward Function	BLEUScore	0.251	0.572	0.603	0.279	1.885	0.283	0.534	0.475	0.287	1.335
	BERTScore	0.259	0.587	0.618	0.291	1.912	0.292	0.540	0.486	0.293	1.380
	Hierarchical Alignment	0.284	0.607	0.626	0.313	2.325	0.298	0.544	0.492	0.299	1.450
Policy Optimization	GRPO	0.263	0.591	0.622	0.305	1.920	0.289	0.538	0.488	0.294	1.395
	CAPO	0.284	0.607	0.626	0.313	2.325	0.298	0.544	0.492	0.299	1.450

Table 6: Comprehensive evaluation of ranking methods, training paradigms, reward functions, and policy optimization on IU-Xray and ReXGradient datasets.

bilizes learning and prevents overconfident updates in critical cases. It produces modest gains over the base model, though performance remains slightly below hierarchical alignment alone. For instance, on MIMIC-CXR, BLEU-2 improves to 0.147 and 1/RadCliQ to 0.815, reflecting safer, more conservative optimization.

The full RadFlow framework, integrating hierarchical alignment, CAPO, and target exploration, achieves the highest overall performance. On CarotidUS-MRG, BLEU-2 reaches 0.522 and BERTScore 0.915, while KeyWordMatch rises to 0.742, illustrating simultaneous improvements in fluency and clinical accuracy. Comparable gains are observed on MIMIC-CXR, IU-Xray, and ReXGradient. These results confirm that the combined design yields synergistic benefits, with target exploration guiding reinforcement updates toward diagnostically weak outputs, hierarchical alignment mitigating reward misalignment, and CAPO ensuring conservative optimization under high-stake conditions.

5.5 Analysis on Target Exploration

Different Ranking Metric Results in Table 5 and Table 6 show that the clinical ranking consistently outperforms single-metric baselines across datasets. On CarotidUS-MRG, the combined clinical ranking achieves KeyWordMatch of 0.742, BLEU-2 of 0.522 and SembScore of 0.891, markedly higher than the BLEUScore-based ranking, which reaches KeyWordMatch of 0.661 and BLEU-2 of 0.478. Similar improvements are observed on MIMIC-CXR, IU-Xray, and ReXGradient, demonstrating the generality of this approach. These results indicate that single-metric ranking, which primarily captures lexical or n-gram similarity, is insufficient for prioritizing diagnostically critical outputs. Our clinical ranking integrates multiple evaluation metrics, including BLEU-2, BERTScore, and RadGraph, capturing both surface-level linguistic quality and clinical consistency. By scoring candidate reports and selecting low-scoring instances for reinforcement fine-tuning, the model focuses on cases where SFT predictions are

incomplete or contain subtle errors. This targeted selection allocates computational resources to high-impact examples, enhancing semantic alignment, diagnostic fidelity, and overall report quality across diverse test sets.

Different Training Paradigm after Sampling The second part of Table 5 and Table 6 illustrates the benefits of reinforcement fine-tuning (RFT) compared with standard supervised fine-tuning (SFT) following Target Exploration. Across all datasets, RFT consistently improves key performance metrics. On MIMIC-CXR, for instance, 1/RadCliQ-v1 increases from 0.902 to 0.939, BLEU-2 from 0.459 to 0.522, BERTScore from 0.321 to 0.401, and SemScore from 0.359 to 0.442. These results demonstrate that RFT effectively leverages diagnostically challenging samples identified through sampling. By focusing updates on cases where SFT outputs are suboptimal, the model refines predictions in a clinically meaningful manner, correcting subtle or underrepresented pathologies, enhancing cross-sectional consistency, and producing Impression sections more aligned with expert annotations. Ranking-guided RFT therefore prioritizes learning on high-impact instances, yielding robust gains in both linguistic quality and clinical accuracy.

5.6 Analysis on Hierarchical Alignment and CAPO

Different Reward Functions Reward design plays a crucial role in shaping model behavior during reinforcement fine-tuning. As shown in the third part of Table 5 and Table 6, the hierarchical alignment reward consistently outperforms single-metric rewards such as BLEUScore or BERTScore. On IU-Xray, for example, hierarchical alignment achieves 1/RadCliQ-v1 of 2.325, BERTScore of 0.607, and SemScore of 0.626, compared with the best single-metric reward (BERTScore) which reaches 1/RadCliQ-v1 of 1.912, BERTScore of 0.587, and SemScore of 0.618, yielding up to a 21.6% improvement in clinical alignment and overall semantic coherence.. The hierarchical reward separates surface-level language fluency from diagnostic content fidelity, aligning the learning objectives with the structured workflow of radiologists. By optimizing both report readability and clinical correctness simultaneously, the model avoids overfitting to superficial n-gram patterns and generates outputs that are coherent and clinically reliable. This reward design encourages cross-sectional consistency between the Findings and Impression sections, mitigates reward hacking, and ensures that diagnostically critical observations are preserved.

Policy Optimization: CAPO vs. GRPO Policy optimization strategy has a significant impact on clinical performance. As shown in Table 5, GRPO achieves 1/RadCliQ-v1 of 1.395, BLEU-2 of 0.289, and BERTScore of 0.538 on RexGradient, whereas CAPO improves all metrics to 1/RadCliQ-v1 of 1.45, BLEU-2 of 0.298, and BERTScore of 0.544. CAPO introduces adaptive, case-specific clipping that constrains policy updates for diagnostically critical reports while allowing more flexible updates for routine cases. This mechanism stabilizes reinforcement fine-tuning by reducing the risk of over correction or hallucination in high-stakes scenarios.

6 Conclusion

In this work, we present a reinforcement fine-tuning framework for medical report generation that integrates ranking-guided sampling with a hierarchical alignment reward. By selectively

focusing on diagnostically challenging cases identified via multi-metric scoring and employing a hierarchical reward that balances linguistic fluency with clinical fidelity, our approach substantially improves both semantic quality and diagnostic accuracy. Extensive experiments on ultrasound and chest X-ray datasets demonstrate consistent gains across different metrics, highlighting the effectiveness of combining targeted exploration, structured reward design, and critical-aware policy optimization.

Despite these improvements, the hierarchical reward relies on handcrafted metrics and may not fully capture deeper clinical reasoning. Future work includes extending the framework to additional imaging modalities such as CT and MRI, incorporating adaptive or learned rewards to better reflect clinical priorities, and integrating human-in-the-loop feedback for real-time refinement. Moreover, leveraging chain-of-thought generation could further align model outputs with structured reporting workflows, ultimately enhancing the reliability and clinical utility of automated medical report generation.

References

- [1] L. H. Schwartz, D. M. Panicek, A. R. Berk, Y. Li, and H. Hricak, “Improving communication of diagnostic radiology findings through structured reporting,” *Radiology*, vol. 260, no. 1, pp. 174–181, 2011.
- [2] D. Ganesan *et al.*, “Structured reporting in radiology,” *Acad. Radiol.*, vol. 25, no. 1, pp. 66–73, 2018.
- [3] B. Jing, P. Xie, and E. Xing, “On the automatic generation of medical imaging reports,” in *Proc. 56th Annu. Meeting Assoc. Comput. Linguistics (ACL)*, Jul. 2018, pp. 2577–2586.
- [4] Y. Li, X. Liang, Z. Hu, and E. P. Xing, “Hybrid retrieval-generation reinforced agent for medical image report generation,” *Adv. Neural Inf. Process. Syst.*, vol. 31, 2018.
- [5] A. Smit, S. Jain, P. Rajpurkar, A. Pareek, A. Ng, and M. Lungren, “Combining automatic labelers and expert annotations for accurate radiology report labeling using BERT,” in *Proc. Empirical Methods Natural Lang. Process. (EMNLP)*, Nov. 2020, pp. 1500–1519.
- [6] Z. Chen, Y. Shen, Y. Song, and X. Wan, “Generating radiology reports via memory-driven transformer,” in *Proc. 59th Annu. Meeting Assoc. Comput. Linguistics and 11th Int. Joint Conf. Natural Lang. Process. (ACL-IJCNLP)*, Nov. 2021, pp. 1439–1449.
- [7] W. Hou, Y. Cheng, K. Xu, W. Li, and J. Liu, “RECAP: Towards precise radiology report generation via dynamic disease progression reasoning,” in *Proc. Conf. Empirical Methods Natural Lang. Process. (EMNLP)*, Dec. 2023, pp. 2134–2147.
- [8] Z. Wang, H. Han, L. Wang, X. Li, and L. Zhou, “Automated radiographic report generation purely on transformer: A multicriteria supervised approach,” *IEEE Trans. Med. Imag.*, vol. 41, no. 10, pp. 2803–2813, Oct 2022.
- [9] S. Yan, W. K. Cheung, K. W. Chiu, T. M. Tong, K. C. Cheung, and S. See, “Attributed abnormality graph embedding for clinically accurate x-ray report generation,” *IEEE Trans. Med. Imag.*, vol. 42, no. 8, pp. 2211–2222, aug 2023.

- [10] Z. Wang, L. Liu, L. Wang, and L. Zhou, “R2gengpt: Radiology report generation with frozen llms,” *Meta-Radiology*, vol. 1, no. 3, p. 100033, 2023.
- [11] C. Pellegrini, E. Özsoy, B. Busam, B. Wiestler, N. Navab, and M. Keicher, “Radialog: Large vision-language models for x-ray reporting and dialog-driven assistance,” in *Proc. Med. Imag. Deep Learn. (MIDL)*, 2025.
- [12] H.-Y. Zhou, J. N. Acosta, S. Adithan, S. Datta, E. J. Topol, and P. Rajpurkar, “Med-versa: A generalist foundation model for medical image interpretation,” *arXiv preprint arXiv:2405.07988*, 2024.
- [13] D. Demner-Fushman *et al.*, “Preparing a collection of radiology examinations for distribution and retrieval,” *Journal of the American Medical Informatics Association*, vol. 23, no. 2, pp. 304–310, 2016.
- [14] A. E. Johnson, T. J. Pollard, S. J. Berkowitz, N. R. Greenbaum, M. P. Lungren, C.-y. Deng, R. G. Mark, and S. Horng, “Mimic-cxr, a de-identified publicly available database of chest radiographs with free-text reports,” *Scientific data*, vol. 6, no. 1, p. 317, 2019.
- [15] X. Zhang, J. N. Acosta, J. Miller, O. Huang, and P. Rajpurkar, “Rexgradient-160k: A large-scale publicly available dataset of chest radiographs with free-text reports,” *arXiv preprint arXiv:2505.00228*, 2025.
- [16] X. Song, X. Zhang, J. Ji, Y. Liu, and P. Wei, “Cross-modal contrastive attention model for medical report generation,” in *Proc. 29th Int. Conf. Comput. Linguist. (COLING)*, 2022, pp. 2388–2397.
- [17] W. Hou, Y. Cheng, K. Xu, Y. Hu, W. Li, and J. Liu, “ICON: Improving inter-report consistency in radiology report generation via lesion-aware mixup augmentation,” in *Findings Assoc. Comput. Linguist.: EMNLP*, Nov. 2024, pp. 9043–9056.
- [18] P. Chambon *et al.*, “Chexpert plus: Augmenting a large chest x-ray dataset with text radiology reports, patient demographics and additional image formats,” *arXiv preprint arXiv:2405.19538*, 2024.
- [19] K. Zhang, Y. Yang, J. Yu, J. Fan, H. Jiang, Q. Huang, and W. Han, “Attribute prototype-guided iterative scene graph for explainable radiology report generation,” *IEEE Trans. Med. Imag.*, vol. 43, no. 12, pp. 4470–4482, dec 2024.
- [20] J. Zhao, Z. Yang, Z. Yang, Z. Chen, H. Fu, and L. Wan, “Topicwise separable sentence retrieval for medical report generation,” *IEEE Trans. Med. Imag.*, vol. 44, no. 3, pp. 1505–1517, mar 2025.
- [21] A. Liu, Y. Guo, J.-H. Yong, and F. Xu, “Multi-grained radiology report generation with sentence-level image-language contrastive learning,” *IEEE Trans. Med. Imag.*, vol. 43, no. 7, pp. 2657–2669, 2024.
- [22] C. Li *et al.*, “Llava-med: Training a large language-and-vision assistant for biomedicine in one day,” *Adv. Neural Inf. Process. Syst.(NIPS)*, vol. 36, pp. 28 541–28 564, 2023.

- [23] H. Liu, C. Li, Q. Wu, and Y. J. Lee, “Visual instruction tuning,” *Adv. Neural Inf. Process. Syst. (NIPS)*, vol. 36, pp. 34 892–34 916, 2023.
- [24] K. Singhal *et al.*, “Large language models encode clinical knowledge,” *Nature*, vol. 620, no. 7972, pp. 172–180, 2023.
- [25] Z. Chen *et al.*, “Chexagent: Towards a foundation model for chest x-ray interpretation,” in *AAAI Spring Symp. Clin. Found. Models*, 2024.
- [26] J. Park *et al.*, “M4cxr: Exploring multitask potentials of multimodal large language models for chest x-ray interpretation,” *IEEE Trans. Neural Netw. Learn. Syst.*, vol. 36, no. 10, pp. 17 841–17 855, 2025.
- [27] X. Zhang, Z. Meng, J. Lever, and E. S. L. Ho, “Libra: Leveraging temporal images for biomedical radiology analysis,” in *Findings of the Association for Computational Linguistics: ACL*, 2025.
- [28] W. Hou *et al.*, “RADAR: Enhancing radiology report generation with supplementary knowledge injection,” in *Proc. 63rd Annu. Meeting Assoc. Comput. Linguist. (ACL)*, Jul. 2025, pp. 26 366–26 381.
- [29] Z. Liu, Z. Sun, Y. Zang, X. Dong, Y. Cao, H. Duan, D. Lin, and J. Wang, “Visual-rft: Visual reinforcement fine-tuning,” *arXiv preprint arXiv:2503.01785*, 2025.
- [30] F. Meng *et al.*, “Mm-eureka: Exploring the frontiers of multimodal reasoning with rule-based reinforcement learning,” *arXiv preprint arXiv:2503.07365*, 2025.
- [31] Q. Yu, Z. Zhang, R. Zhu, Y. Yuan, X. Zuo, Y. Yue, W. Dai, T. Fan, G. Liu, L. Liu *et al.*, “Dapo: An open-source llm reinforcement learning system at scale,” *arXiv preprint arXiv:2503.14476*, 2025.
- [32] C. Zheng, S. Liu, M. Li, X.-H. Chen, B. Yu, C. Gao, K. Dang, Y. Liu, R. Men, A. Yang *et al.*, “Group sequence policy optimization,” *arXiv preprint arXiv:2507.18071*, 2025.
- [33] C. Liu, H. Wang, J. Pan, Z. Wan, Y. Dai, F. Lin, W. Bai, D. Rueckert, and R. Arcucci, “Beyond distillation: Pushing the limits of medical llm reasoning with minimalist rule-based rl,” *arXiv preprint arXiv:2505.17952*, 2025.
- [34] X. Zhang, Y. Wang, Z. Feng, R. Chen, Z. Zhou, Y. Zhang, H. Xu, J. Wu, and Z. Liu, “Medu1: Incentivizing unified medical reasoning in llms via large-scale reinforcement learning,” *arXiv preprint arXiv:2506.12307*, 2025.
- [35] J. Pan *et al.*, “MedVLM-R1: Incentivizing Medical Reasoning Capability of Vision-Language Models (VLMs) via Reinforcement Learning,” in *Proc. Med. Image Comput. Comput.-Assist. Intervent. (MICCAI)*, vol. LNCS 15966, September 2025.
- [36] Y. Lai, J. Zhong, M. Li, S. Zhao, and X. Yang, “Med-r1: Reinforcement learning for generalizable medical reasoning in vision-language models,” *arXiv preprint arXiv:2503.13939*, 2025.

- [37] G. Liu *et al.*, “Clinically accurate chest x-ray report generation,” in *Proc. Machine Learning Healthc.(PMLR)*, 2019, pp. 249–269.
- [38] S. Yang, X. Wu, S. Ge, Z. Zheng, S. K. Zhou, and L. Xiao, “Radiology report generation with a learned knowledge base and multi-modal alignment,” *Medical Image Analysis*, vol. 86, p. 102798, 2023.
- [39] X. Yi, Y. Fu, J. Yu, R. Liu, H. Zhang, and R. Hua, “Lhr-rfl: Linear hybrid-reward-based reinforced focal learning for automatic radiology report generation,” *IEEE Trans. Med. Imag.*, vol. 44, no. 3, pp. 1494–1504, 2025.
- [40] K. Papineni, S. Roukos, T. Ward, and W.-J. Zhu, “Bleu: a method for automatic evaluation of machine translation,” in *Proceedings of the 40th annual meeting of the Association for Computational Linguistics*, 2002, pp. 311–318.
- [41] T. Zhang*, V. Kishore*, F. Wu*, K. Q. Weinberger, and Y. Artzi, “Bertscore: Evaluating text generation with bert,” in *International Conference on Learning Representations*, 2020.
- [42] S. Jain, A. Agrawal, A. Saporta, S. Q. Truong, D. N. Duong, T. Bui, P. Chambon, Y. Zhang, M. P. Lungren, A. Y. Ng *et al.*, “Radgraph: Extracting clinical entities and relations from radiology reports,” *arXiv preprint arXiv:2106.14463*, 2021.
- [43] A. Hurst, A. Lerer, A. P. Goucher, A. Perelman, A. Ramesh, A. Clark, A. Ostrow, A. Welihinda, A. Hayes, A. Radford *et al.*, “Gpt-4o system card,” *arXiv preprint arXiv:2410.21276*, 2024.
- [44] X. Zhang, H.-Y. Zhou, X. Yang, O. Banerjee, J. N. Acosta, J. Miller, O. Huang, and P. Rajpurkar, “Rexrank: A public leaderboard for ai-powered radiology report generation,” *arXiv preprint arXiv:2411.15122*, 2024.
- [45] F. Yu *et al.*, “Evaluating Progress in Automatic Chest X-Ray Radiology Report Generation,” *Radiology and Imaging*, Tech. Rep., Aug. 2022.
- [46] C. Wu, X. Zhang, Y. Zhang, H. Hui, Y. Wang, and W. Xie, “Towards generalist foundation model for radiology by leveraging web-scale 2d&3d medical data,” *Nature Communications*, vol. 16, no. 1, p. 7866, 2025.